Development of a momentum microscope for time resolved band structure imaging

B. Krömker,[1] M. Escher,[2] D. Funnemann,[1] D. Hartung,[3] H. Engelhard,[3] and J. Kirschner[3]
[1]*Omicron Nanotechnology GmbH, 65232 Taunusstein, Germany*
[2]*Focus GmbH, 65510 Hünstetten, Germany*
[3]*Max-Planck-Institut für Mikrostrukturphysik, 06120 Halle, Germany*

(Received 6 February 2008; accepted 9 April 2008; published online 19 May 2008)

We demonstrate the use of a novel design of a photoelectron microscope in combination to an imaging energy filter for momentum resolved photoelectron detection. Together with a time resolved imaging detector, it is possible to combine spatial, momentum, energy, and time resolution of photoelectrons within the same instrument. The time resolution of this type of energy analyzer can be reduced to below 100 ps. The complete ARUPS pattern of a Cu(111) sample excited with He I, is imaged in parallel and energy resolved up to the photoelectron emission horizon. Excited with a mercury light source ($h\nu$=4.9 eV), the Shockley surface state at the energy threshold is clearly imaged in k-space. Electron-electron interactions are observed in momentum space as a correlation hole in two-electron photoemission. With the high transmission and the time resolution of this instrument, possible new measurements are discussed: Time and polarization resolved ARUPS measurements, probing change of bandstructure due to chemical reaction, growth of films, or phase transitions, e.g., melting or martensitic transformations. © *2008 American Institute of Physics.*
[DOI: 10.1063/1.2918133]

I. INTRODUCTION

Our aim is to image the complete momentum distribution of photoexcited electron states in an energy plane through the Brillouin zone. The basic idea is to project the momentum image from the back focal plane of the objective lens of a photoelectron emission microscope (PEEM) through an energy filter onto an image detector. This concept dates back to the middle of the last century, for a review, see Bauer.[1] Since for imaging the angular distribution of photoelectrons energy filtering is mandatory, various types of filters have been used: time-of-flight systems,[2] deflection in an electrostatic field,[3] a mulitpole Wien filter,[4] or filtering in a planar retarding field.[5] Our design is based on a modified NanoESCA integrating a PEEM with an imaging energy filter. The spherical (α^2) aberrations are strongly reduced by a novel analyzer design. A mostly aberration-free and energy filtered image of the electrons angular distribution emanating from an adjustable sample area of up to 100 μm diameter appears at the detector. The projected image displays the $E(k)$ band structure of the photoelectrons within a momentum plane of constant kinetic energy. The full valence band can be observed by an energy sequence of parallel cuts through the Brillouin zone. Data acquisition is fast due to the simultaneous detection of all electrons within a given energy window. Complete momentum planes can be obtained within a couple of minutes with a standard discharge laboratory source (He I). As an example, photoemission measurements of a Cu(111) surface are shown. In a further step, the use of a delay line detector instead of a luminescence screen allows to detect electron coincidences. We show that the time dispersion of the electron trajectories through this energy analyzer is considerably less than in conventional hemispherical analyzers. The smaller time dispersion allows to obtain a better discrimination of the true coincidences from statistical ones.

II. INSTRUMENT

The instrument used is based on a NanoESCA photoemission spectrometer comprising a PEEM column and a double hemispherical imaging energy filter. The aberrations of the first hemispherical analyzer are compensated with the help of a second hemisphere, such that the inner electron trajectories in the first hemisphere become the outer trajectories in the second hemisphere.

A. Imaging microscope

The imaging quality achieved by the combination of a PEEM lens with the imaging double hemispherical analyzer has been demonstrated with ultraviolet photoelecton spectroscopy and x-ray photoelectron spectroscopy (XPS) imaging.[6] In soft XPS, a lateral resolution of 150 nm was achieved.[7] With a photon energy of 4.9 eV, energy filtered images of polycrystalline copper grains were measured with a lateral resolution of 40 nm.[8]

B. Time resolution

According to Fermat's principle, a good imaging quality results in an extremal time of electron pulses when traveling through the electron optics. This comprises the lens as well as the energy analyzer. As mentioned above, we implemented an aberration compensated hemispherical analyzer. This also implies that the transit time jitter is largely compensated. For a given energy, an electron may travel on an

outer orbit in the first hemisphere because of its starting angle and then travels on an inner orbit in the second hemisphere because of the field symmetry. The travel time for an electron starting on an inner orbit and finishing on an outer will be the same. In a conventional hemispherical analyzer, the travel time for electrons with different entrance angles will be different. The time spread after a revolution of 180 ° in a hemispherical analyzer is given by Imhof.[9] Up to first order in slit width d and entrance angle α,

$$\frac{\Delta T}{T_{180°}} \cong \frac{3}{2}\frac{d}{R_0} + \frac{8}{\pi}\alpha, \tag{1}$$

$T_{180°}$ is the transit time of a particle with the pass energy E_0 traveling in a semicircle of radius R_0. For an imaging double hemispherical analyzer, the achievable time resolution was derived by Funnemann.[10] The transit time T for a complete ellipsoidal trajectory of a particle with energy E is independent of the start angle[11] α,

$$T = \text{const}\, E^{-3/2}. \tag{2}$$

Particles with a small energy difference dE arrive with a time difference dT according to

$$\frac{dT}{T} = -\frac{3}{2}\frac{dE}{E}. \tag{3}$$

The energy resolution term on the right side is well known from the literature[12] and can be applied because this analyzer uses energy resolving slits just as an hemispherical analyzer.

$$\frac{\Delta E}{E_0} = \frac{d}{2R_0} + \alpha^2. \tag{4}$$

By using small slits and a small entrance angle as a good approximation, we replace the general time T by the time required for a full circular orbit $T_{360°}$ and use the pass energy E_0. The relative time spread can be calculated as a function of geometrical parameters,

$$\frac{\Delta T}{T_{360°}} \cong -\frac{3}{2}\left[\frac{d}{2R_0} + \alpha^2\right]. \tag{5}$$

For a pass energy of 100 eV, the transit time is $T_{360°} = 186$ ns. For a slit width of $d = 0.5$ mm, a radius of 124 mm, and an entrance angle of $\alpha = 1.5°$, the calculated time spread is $\Delta T \approx 0.5$ ns (base width). For the same parameters, the time spread of an hemispherical analyzer was calculated to be 5 ns. Choosing a higher pass energy, a smaller slit width and a smaller angular acceptance can improve the time resolution further to below 100 ps.

C. Momentum microscope

Figure 1 shows the electron optical elements and schematical electron trajectories of the lens in both modes: spatial imaging [Fig. 1(a)] and angular resolved k-space imaging [Fig. 1(b)]. An important design concept of this instrument is the ability to switch between spatial and momentum imaging. Switching between the two modes keeps the position of the first real image in the field aperture and the position of the k-space image in the contrast aperture, so that the positions of the apertures, deflectors, and stigmators are well adapted for both cases. In each case, schematic electron trajectories for three different sample positions and angles are shown. Photoelectrons from the sample are extracted by a voltage of up to 15 kV. For low kinetic energies, the full angular range of ±90° can be imaged. A contrast aperture located in the back focal plane, adjustable in size and position, limits the angular range transmitted, and improves the spatial resolution. For angular resolved mode, the contrast aperture is fully opened to transmit a large angular range (i.e., large k-space). In this mode, the size of the field aperture controls the k-space resolution. In both cases, the first intermediate image is located at the position of the field aperture.

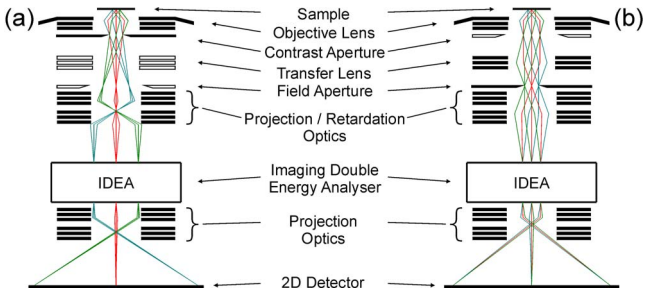

FIG. 1. (Color online) (a) Schematic view of the lens optics of the real space imaging NanoESCA compared to (b) the lens optics of the momentum microscope for k-space imaging.

In the angular resolved mode, a transfer lens is switched on in order to decrease the lateral magnification in the first image plane. According to Helmholtz Lagrange law, a decrease of the lateral magnification increases the angular magnification. A continuously adjustable field aperture confines the spatial area at the sample that is used for the angular image. The achievable k-space resolution is a function of the field of view and depends on the energy resolution. See calculated data in Fig. 2.

The projection and retardation optics transfer either the real space image from the position of the field aperture or the k-space image from the position of the back focal plane into the entrance of the energy analyzer. The analyzer transfers an

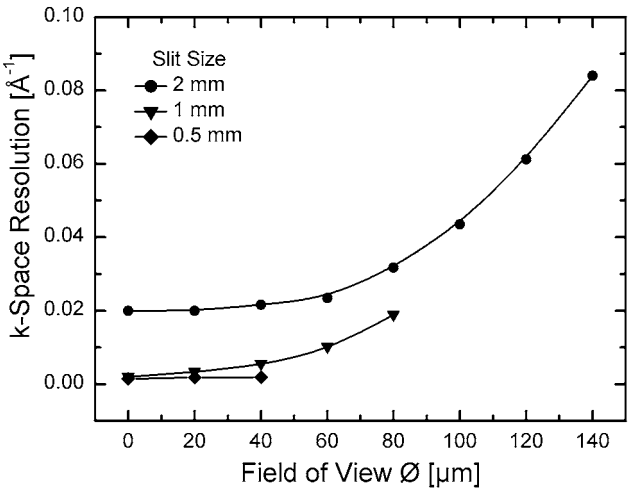

FIG. 2. Instrumental k-space resolution (base width) depending on the field of view at the sample calculated for electrons with a kinetic energy of 15 eV and an analyzer pass energy of 100 eV. Diffraction effects which change the resolution for small field of views ($\ll 10$ μm) are not taken into account.

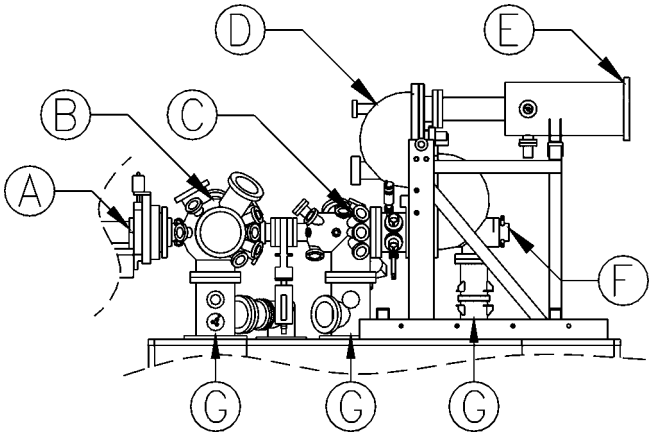

FIG. 3. Side view of the momentum microscope with preparation and analysis chamber. (A) Nitrogen cooled, rotatable sample manipulator, (B) preparation chamber equipped with Auger spectrometer, MEED, sputter ion source and e-beam evaporator, (C) analysis chamber with PEEM lens, helium discharge lamp and mercury UV-source, (D) aberration corrected energy filter, (E) luminescence screen with CCD camera or delay line detector, (F) luminescence screen for PEEM mode, and (G) pumping.

energy filtered image to its exit with unity magnification. A set of lenses projects the magnified image onto a two dimensional (2D) detector, which consists either of a stack of a channel plate and a luminescence screen or a delay line detector. The analyzer was operated with pass energies of 50 and 100 eV and slit settings of 0.5, 1, and 2 mm width. For these settings, the calculated instrumental energy resolution is between 70 meV and 0.5 eV [full width at half maximum-(FWHM)]. When the analyzer is switched off (not shown in the lens optics diagram), the lenses project the image without retardation through a hole in the outer hemisphere of the first energy analyzer on a luminescence screen for PEEM mode imaging.

Figure 3 shows a side view of the momentum microscope. The instrument is designed for preparation of single crystals and a quick and reliable transfer from the preparation to the analysis chamber. The sample can be cooled on the sample manipulator with liquid nitrogen and heated up to 600 °C.

III. EXPERIMENTAL RESULTS

Figure 4 shows *k*-space images of a Cu(111) single crystal taken with photon energies of 4.9 and 21.2 eV. The kinetic energy of the electrons imaged with the mercury UV source is close to zero which results in a small diameter of the *k*-space horizon.[13] This is the maximum momentum of electrons parallel to the surface, i. e., of those leaving the sample parallel to the surface. The surface state of Cu(111) can be clearly seen as a bright circle in Fig. 4(a). This is the first time this surface state is imaged in *k*-space with a photon energy as low as 4.9 eV. An image with E_B=3 eV taken at the photon energy of 21.2 eV [Fig. 4(b)] shows the threefold symmetry of the bulk (111) orientation. A sharp dark line structure (crossing the line CD) in the high intensity range of the *d*-states was used to optimize the lens settings of the microscope. The band structure of copper is well known,[13] and the photoelectrons from its Fermi surface have

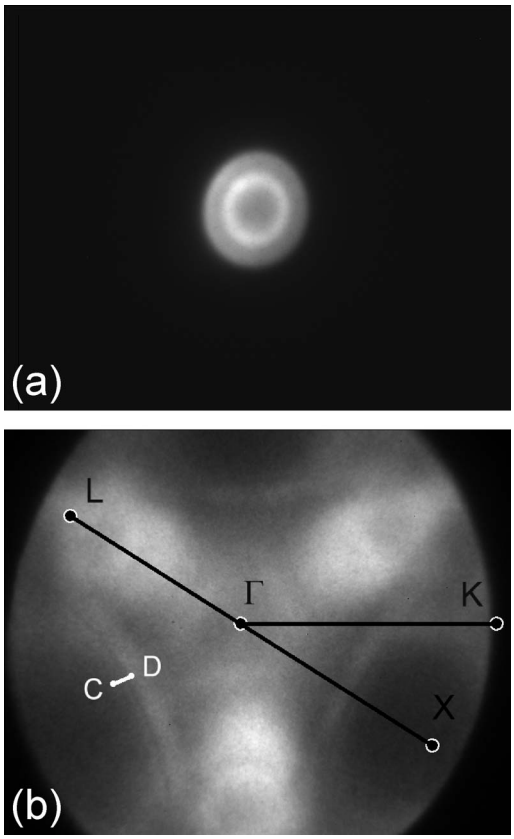

FIG. 4. Intensity distributions with a linear gray scale of photoelectron momenta from a Cu (111) sample. The scaling of the parallel momentum is the same in both images. Note the increase of the diameter of the photoemission horizon for electrons with higher kinetic energy from image [(a) and (b)]. (a) Fermi map excited with a photon energy of $h\nu$=4.9 eV (mercury UV source), exposure time of 3 s. (b) Copper 3*d* electrons at E_B=3 eV, excited with $h\nu$=21.2 eV, exposure time of 5 min. The black capital letters indicate the directions of high symmetry. The distance *L*–*X* has a length of 3.08 Å^{-1}. A line scan CD across the thin dark line is shown in Fig. 6(b).

been previously imaged with good resolution and at low temperature.[14] Therefore, the imaging of the *k*-space at the Fermi energy and the band structure $E(k)$ at higher binding energies is a good test to characterize the momentum microscope.

In Fig. 5, the Fermi map excited by the He I source (21.2 eV) is displayed with a logarithmic intensity scale. The image was taken within 5 min in one exposure with the camera background subtracted. The energy resolution of the analyzer was selected by using a slit width of 0.5 mm and a pass energy of 100 eV which resulted in a measured energy resolution of 0.2 eV (see Fig. 8). The black hexagon indicates the surface Brillouin zone. The distance $\overline{MM'}$=2.84 Å^{-1} taken from literature is used for scaling the *k*-space image. The rectangular limits of the image are imposed by the size of the detector chip in the charge coupled device (CCD) camera. The black lines at the four corners indicate the rim of the luminescence screen. To estimate the experimental resolution in *k*-space, line scans of sharp features were taken. Figure 6 shows the intensity as a function of *k* (line AB in Fig. 5) at the Fermi energy and in the *d*-band region (along line CD in Fig. 4). The FWHM of 0.08 Å^{-1} can be compared to a similar feature measured by Kotsugi *et al.*[5] We measured

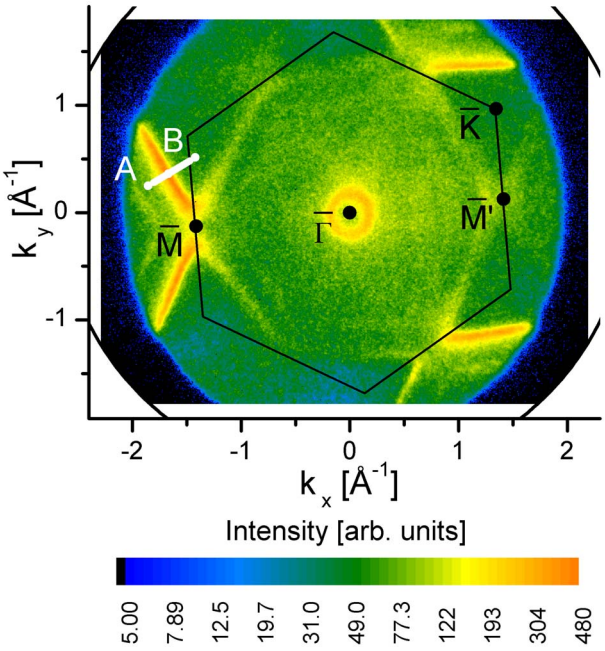

FIG. 5. (Color online) *k*-space image of Cu (111) taken at the Fermi energy with an exposure time of 5 min excited with He I. The intensity is scaled logarithmic. The small ring in the center is the Shockley surface state. The surface Brillouin zone is marked by a black hexagon. The photoemission horizon limits the circular central area with a radius of about 2 $Å^{-1}$. Outside this radius the screen is dark. The black lines at the corners mark the diameter of the luminescence screen. An intensity profile along *k*-space direction AB is shown in Fig. 6(b).

a half width of about a factor of 2 smaller than the previously reported one. The sharpest *k*-space feature we found in the energy range of the copper *d*-bands [Fig. 6(b)] shows a resolution of 0.034 $Å^{-1}$ (FWHM). The intrinsic *k*-space peak width is influenced by the band structure, especially the lifetime and group velocities of the bands involved in the transition. Therefore, the instrumental broadening is rather smaller than the measured width.

In Fig. 5, the intensity drop off outside the central circular area is the photoemission horizon at this photon energy.[15] The radius in *k*-space depends on the kinetic energy probed. Outside the crystal, the maximum $k_{\|}$ radius is calculated from $E_{\mathrm{kin,max}}=(\hbar^2 k_{\|\mathrm{max}}^2)/2m_e$. At the Fermi edge, the kinetic energy is calculated with $E-E_F=21.2$ eV from $E_{\mathrm{kin}}=E-E_F-e\Phi$. The literature work function of $e\Phi=4.9$ eV must be corrected by 0.1 eV for the Schottky effect to an effective work function of 4.8 eV, which results in $E_{\mathrm{kin}}=16.4$ eV. The calculated maximum *k* value of

$$k_{\|\mathrm{max}}(Å^{-1}) = 0.5124\sqrt{E_{\mathrm{kin,max}}(eV)} = 2.07\ Å^{-1} \tag{6}$$

matches the scaling in Fig. 5 derived from literature data.

Figure 7 shows that the radius of *k*-space intensity distribution varies with energy $E_{\mathrm{kin}} \propto k_{\|}^2$ as expected. The intensity distribution shows that one can easily measure down to zero kinetic energy. The work function of the sample can be experimentally determined. The work function measured here is $e\Phi=4.7$ eV probably due to contamination from the residual gas or from impurities in the He flow from the discharge lamp.

Images taken at successive energies can be stacked to a data cube. From this, cuts in different planes or along lines arbitrarily chosen can be selected. Figure 8 shows an intensity distribution for normal emission. A fit at the Fermi edge to derive the energy broadening has to include the surface state. A total energy width of $\Delta E=200$ meV (FWHM) was measured. Taking into account the room temperature broadening of $\Delta E=100$ meV (FWHM), the instrumental energy resolution is $\Delta E_{\mathrm{inst}}=170$ meV (FWHM).

Cutting the stack of images in a high symmetry direction, the angular distribution of the emitted electrons is visualized showing the band structure. An example is shown in Fig. 9.

IV. OUTLOOK

A. Speed

The parallel detection scheme employed here provides enormous gains in data flow as compared to conventional analyzers, even if they have parallel energy detection at the output. The *K*-space intensity maps at constant energy take about 10 s/frame with an ordinary laboratory light source. Note that raw data are shown; no symmetry averaging or energy correction has been applied. Such order-of-magnitude gains may enable qualitatively new studies. The changes of a band structure in real time upon irreversible processes such as reactions with chemically active gases or deposition of metal atoms and growth of films can be studied. An experiment with a resolution of percents of a monolayer could be performed in a day in the laboratory or in a couple of hours at a synchrotron radiation source. Likewise, one may follow

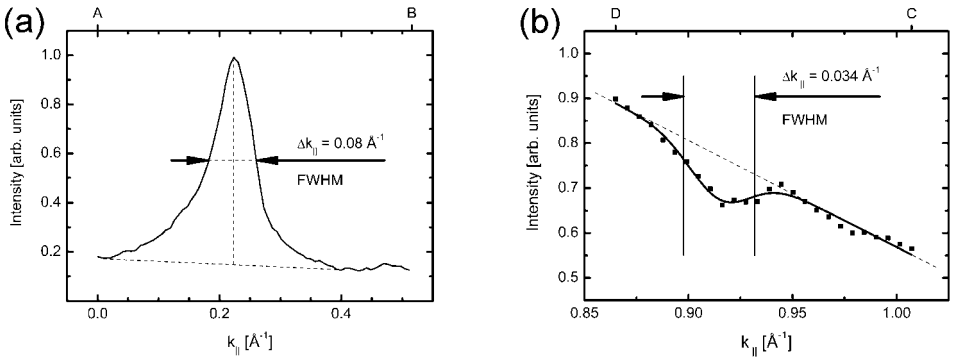

FIG. 6. Intensity profiles from *k*-space. (a) Profile along the line AB as indicated in Fig. 5. The peak maximum is at a distance $k_{\|}$ of 1.71 $Å^{-1}$ from Γ corresponding to an angle outside the crystal of $\Theta=56°$ of the electron trajectory. The width of the structure is $\Delta k_{\|}=0.08$ $Å^{-1}$ FWHM. (b) Intensity profile along the line DC as indicated in Fig. 4(b). To estimate the *k*-space resolution, the intensity profile is fitted with a linear and a Gaussian function as shown. The width of the Gaussian is $\Delta k_{\|}=0.034$ $Å^{-1}$ FWHM.

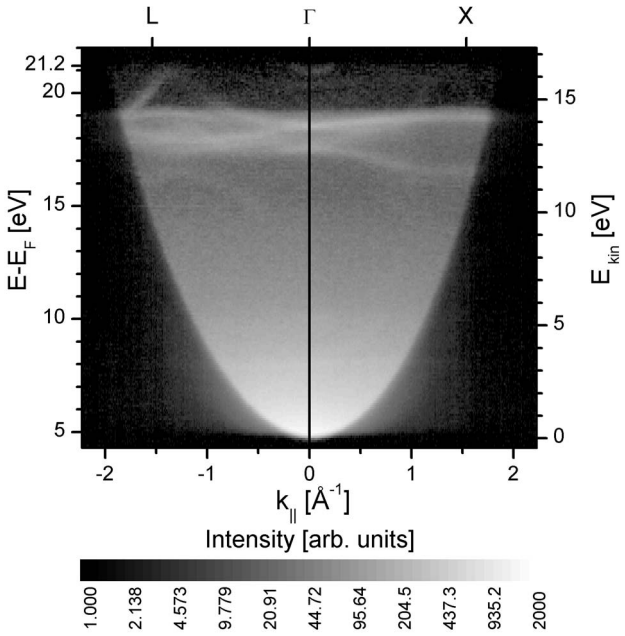

FIG. 7. Band structure in the direction $L\Gamma X$. The energy dispersion $E \sim k^2$ can be easily seen at the photoemission horizon. The full range from zero kinetic energy is visible. To generate this display, a stack of 183 images was acquired with an exposure time of 10 s each. The energy step between the images was $dE=0.1$ eV, pass energy of 100 eV, slit width of 0.5 mm, and photon energy 21.2 eV (He I). From the three dimensional data cube, a section in $L\Gamma X$ direction is generated. The intensity is displayed on a logarithmic scale.

the effects of slow heating and cooling in real time on the valence band momentum distribution of alloys, at order-disorder transitions, perhaps even melting.

Modern synchrotron radiation sources offer orthogonal beam polarizations in two beams which are alternately blanked at a frequency of 1–100 Hz. The light polarization gives rise to selection rules in the contour maps and to dichroism effects of various kinds.[16] With a chopper and synchronous gating of the image detection, the dynamical evolution of dichroism in *K*-space, e. g., while approaching a Curie or Néel temperature is experimentally accessible.

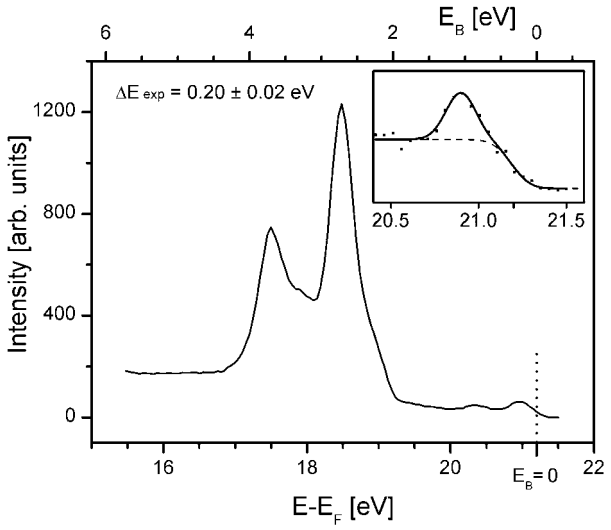

FIG. 8. Intensity vs energy along normal emission integrated over a range of $\Delta k_{\|} = \pm 0.1$ Å^{-1}. The insert shows the Fermi edge region with an integration range of $\Delta k_{\|} = \pm 0.01$ Å^{-1}. The width of the Fermi edge is measured to be 0.2 eV (12%–88% of height, corresponding to FWHM of the integrated Gaussian).

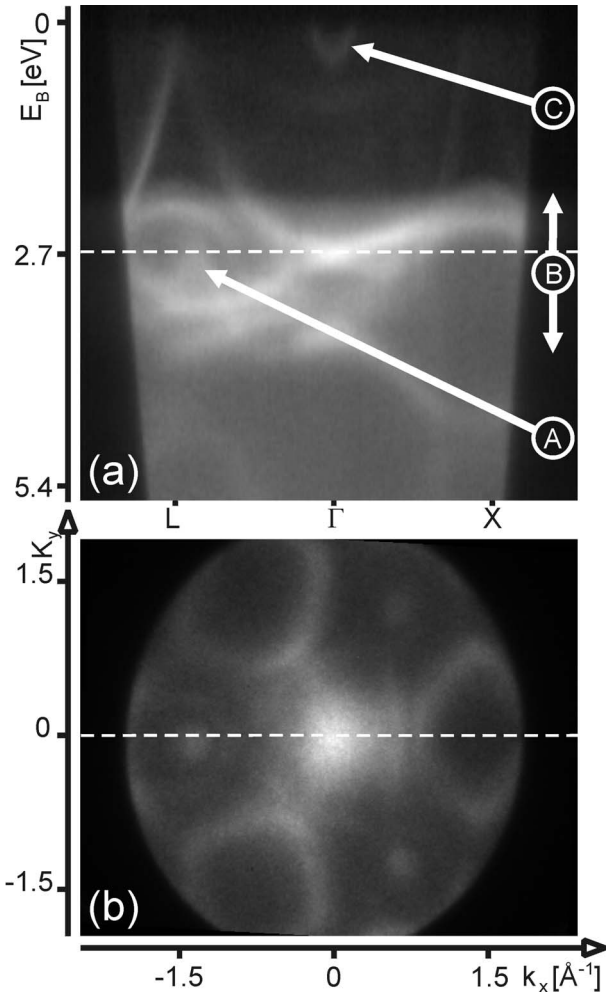

FIG. 9. Band structure map derived from a cut through a measured data cube $I(E_B,k_x,k_y)$. (a) Band structure $I(E_B,k_x)$ along the line $L\Gamma X$. (A) Tamm surface state, (B) range of 3*d* bands, and (C) Shockley surface state. The dashed white line corresponds to the cut through the data cube shown in part (b). Intensity distribution of the 3*d* orbitals as function of k_x,k_y at a binding energy of 2.7 eV.

B. Energy range

The present instrument is designed to analyze photoelectrons up to 1.6 keV. The momentum imaging is by no means restricted to the valence band regime. Core level photoelectrons also experience diffraction by neighboring atoms. Together with modern computational codes,[17] this leads to element specific structural information of high quality if the photoelectron diffraction patterns are accurately measured and over a large angular range. This could be achieved with the present momentum microscope.

The primary excitation source is preferably not a charged particle because of the high field in front of the sample. An alternative source of energy to emit electrons would be the potential energy of highly excited atoms.[18] The angular distribution of ejected electrons upon the approach of such atoms has not been studied in detail, the existence of momentum selected "bands" is presently unknown. This

holds for the whole possible potential energy range of highly excited atoms in the energy range from eV to keV, depending on the atomic species and its excitation state.

C. Time resolution

In double photoemission (see below), we found a time spread of 2 ns FWHM for coincident electrons. This includes the time of creation of a pair (<10 fs), the transit time spread through the PEEM optics (≈100 ps), the time spread through the analyzer, the transit time through the projection stage and the time resolution of the electronics of the 2D detector. While none of these contributions were individually measured, it is reasonable to assume that a time resolution of the order of 1 ns is achievable. This opens the way to another class of experiments: observing the reversible changes of the electronic structure by means of stroboscopic techniques with a time resolution in the order of nanoseconds. One may, e. g., excite a sample with an intense laser pulse and delayed by a nanosecond or a millisecond, send in a short UV or x-ray light pulse to probe the actual bandstructure at this point of time. This process may be repeated in the usual way. A possible application would be to follow the Baines path in martensitic transformations.

D. Double photoemisson

One photon may occasionally create two electrons simultaneously.[19] This is not explainable within the common theories of photoemission employing the dipole approximation, but in agreement with Einstein's second law of photoemission.[20] Both kinetic energies together plus twice the work function equal the photon energy. Such a process occurs on a time scale of less than a femtosecond in a spatial region of about a lattice constant. The two liberated electrons interact with each other by Coulomb and by exchange interaction. The net effect is that they repel each other from the beginning and try to keep their trajectories apart. The physics of interest is this zone of avoidance of each two electrons because this is at the bottom of the "exchange-correlation hole," a concept of utmost importance in physics and chemistry.[21] The requirements needed for doing experiments are energy resolution, angular resolution, and time resolution. As mentioned above, such an electron pair arrives at the detector within 1 ns, which greatly helps to discriminate against another accidental pair which arrives within, say, 10 ns. Finally, a detector must exist which allows to detect two electrons arriving at the same time in different locations. This can be done with a delay-line detector.[22] The 2D detector then displays the points of impact of each electron pair. If one fixes the momentum of the one electron within a certain region of interest, the probability of the second electron to land within a certain radius can be read from the intensity distribution. The result of such an experiment with Cu(111), excited by He II at an energy in the *d*-band region is seen in Fig. 10. There are three intensity lobes, similar to those in Fig. 4, demonstrating that even a two-electron state may have a well-defined momentum. One of the lobes is not visible—we placed our region of interest on it. The complete suppression of any second electron arriving at or near the first electron is the key observation of this experiment. The present instrument is a very good tool to study the emission of electron pairs correlated in time, space, and energy.

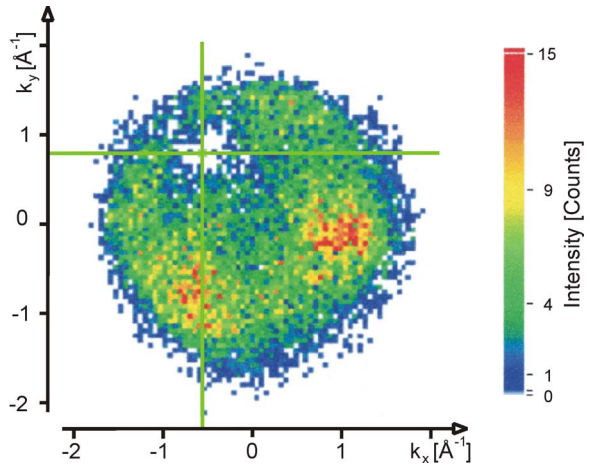

FIG. 10. (Color online) *k*-space resolved coincidence intensity of electron pairs excited with $h\nu$=40.8 eV originating from Cu (111) with $E_B \sim 3$ eV. The energy resolution in this image was ΔE=0.5 eV FWHM. Using the delay line detector the lateral coordinates k_x, k_y, and the time is recorded. The coincidence counts are displayed with reference to electrons detected at the cursor position marked by the green cross hair. By setting the acceptance time interval for the second electron to 3 ns (base width) with respect to the initial electron at the cursor position, the noncorrelated count rate is suppressed. A minimum of the coincidence intensity is observed around the *k*-space position where the first electron was emitted. A maximum of the correlated photoelectron intensity is found at two other symmetry equivalent directions. This image can be compared to Fig. 4(b), showing the *k*-space map of the single photoelectrons.

ACKNOWLEDGMENTS

We like to thank Dr. O. Renault from CEA-LETI, MINATEC for the loan of the well polished, and preoriented polycrystalline copper sample used during the prealignment of the instrument.

[1] E. Bauer, J. Electron Spectrosc. Relat. Phenom. **114**, 975 (2001).
[2] G. Schönhense, A. Oelsner, O. Schmidt, G. H. Fecher, V. Mergel, O. Jagutzki, and H. Schmidt-Böcking, Surf. Sci. **480**, 180 (2001).
[3] B. P. Tonner, D. Dunham, T. Droubay, and M. Pauli, J. Electron Spectrosc. Relat. Phenom. **84**, 211 (1997).
[4] H. Niimi, M. Kato, T. Tsutsumi, T. Kawasaki, H. Matsudaira, S. Suzuki, W.-J. Chun, Y. Kitajima, M. Kudo, and K. Asakura, Appl. Surf. Sci. **241**, 131 (2005).
[5] M. Kotsugi, W. Kuch, F. Offi, L. I. Chelaru, and J. Kirschner, Rev. Sci. Instrum. **74**, 2754 (2003).
[6] M. Escher, N. Weber, M. Merkel, C. Ziethen, P. Bernhard, G. Schönhense, S. Schmidt, F. Forster, F. Reinert, B. Krömker, and D. Funnemann, J. Phys.: Condens. Matter **17**, S1329 (2005).
[7] O. Renault, N. Barrett, A. Bailly, L. F. Zagonel, D. Mariolle, J. C. Cezar, N. B. Brookes, K. Winkler, B. Krömker, and D. Funnemann, Surf. Sci. **601**, 4727 (2007).
[8] O. Renault, R. Brochier, A. Roule, P.-H. Haumesser, B. Krömker, and D. Funnemann, Surf. Interface Anal. **38**, 375 (2006).
[9] R. E. Imhof, A. Adams, and G. C. King, J. Phys. E **9**, 138 (1976).
[10] D. Funnemann (unpublished).
[11] L. D. Landau and E. M. Lifschitz, *Lehrbuch der Theoretischen Physik* (Akademie, Berlin, 1976), p. 44.
[12] D. Roy and J. D. Carette, in *Electron Spectroscopy for Surface Analysis*, edited by H. Ibach (Springer, Berlin, 1977), p. 13.
[13] R. Matzdorf, Surf. Sci. Rep. **30**, 153 (1998).
[14] F. Baumberger, A. Tamai, M. Muntwiler, T. Greber, and J. Osterwalder, Surf. Sci. **532**, 82 (2003).

[15] T. Greber, Lect. Notes Phys. **94**, 580 (2001).
[16] S. Schmidt, N. Weber, H.-J. Elmers, F. Forster, F. Reinert, S. Hüfner, M. Escher, M. Merkel, B. Krömker, and D. Funnemann, Phys. Rev. B **72**, 064429 (2005).
[17] A. Winkelmann, B. Schröter, and W. Richter, J. Phys.: Condens. Matter **16**, S1555 (2004).
[18] W. Sesselmann, B. Woratschek, J. Küppers, G. Ertl, and H. Haberland, Phys. Rev. B **35**, 8348 (1987); P. Ferro, R. Moroni, M. Salvietti, M. Canepa, and L. Mattera, Surf. Sci. **407**, 212 (1998).
[19] R. Hermann, S. Samarin, H. Schwabe, and J. Kirschner, Phys. Rev. Lett. **81**, 2148 (1998).
[20] A. Einstein, Ann. Phys. **17**, 132 (1905).
[21] F. O. Schumann, C. Winkler, C. Kerherve, and J. Kirschner, Phys. Rev. B **73**, 041404 (2006); F. O. Schumann, C. Winkler, and J. Kirschner, New J. Phys. **9**, 372 (2007); F. O. Schumann, C. Winkler, and J. Kirschner, Phys. Rev. Lett. **98**, 257604 (2007).
[22] O. Jagutzki, V. Mergel, K. Ullmann-Pfleger, L. Spielberger, U. Spillmann, R. Dörner, and H. Schmidt-Böcking, Nucl. Instrum. Methods Phys. Res. A **477**, 244 (2002).